Article

A Novel LQI Control Technique for Interleaved-Boost Converters

Eiichi Sakasegawa [1,*], So Watanabe [1], Takayuki Shiraishi [1], Hitoshi Haga [2] and Ralph M. Kennel [3]

1   National Institute of Technology, Kagoshima College, 1460-1, Kirishima 899-5193, Kagoshima, Japan; swatanab@kagoshima-ct.ac.jp (S.W.); shiraishi@kagoshima-ct.ac.jp (T.S.)
2   Department of Electrical and Electronics Engineering, Shizuoka University, Hamamatsu 432-8561, Shizuoka, Japan; haga.hitoshi@shizuoka.ac.jp
3   TUM School of Engineering and Design Department of Energy and Process Engineering, Technical University of Munich, Arcisstrasse 21, 80333 Munich, Germany; ralph.kennel@tum.de
*   Correspondence: sakasegw@kagoshima-ct.ac.jp

Abstract: Hybrid electric vehicles (HEVs) and fuel cell electric vehicles (FCEVs) utilize boost converters to gain a higher voltage than the battery. Interleaved boost converters are suitable for low input voltage, large input current, miniaturization, and high-efficiency applications. This paper proposes a novel linear quadratic integral (LQI) control for the interleaved boost converters. First, the small-signal model of the interleaved-boost converter is derived. In the proposed method, an output voltage and a current signal error between two-phase input currents are selected to control not only the output voltage but also a balance between two-phase input currents. Furthermore, steady-state characteristics in terms of the output voltage and the input current are demonstrated by experiments and simulations using an experimental apparatus with a rated power of 700 W. The validity of the proposed method's tracking performance and load response is demonstrated by comparing it with that of the conventional PI control. The tracking performance of the LQI control for the 40 V step response has a ten times faster response than that of the PI control. Also, the experimental results demonstrate that the proposed method maintains a constant output voltage for a 300 W load step while the PI control varies by 10 V during 70 ms. Additionally, the proposed method has an excellent disturbance rejection.

Keywords: EV; HEV; interleaved boost converter; LQI control; optimal regulator; small-signal-model

1. Introduction

CO_2 reduction is the biggest challenge in the world, and automobiles play an important role [1]. DC link voltage variable systems with DC/DC converters are used in hybrid electric vehicles (HEVs) and fuel cell electric vehicles (FCEVs) [2]. Interleaved-boost converters can increase power capability and overall switching frequency by using interleaved switching, a well-known concept of sequential switching. Therefore, interleaved-boost converters have been widely studied for automobiles and industry applications such as grid systems. For example, reference [3] reports a boost converter with a coupled inductor and a common clamping capacitor capable of high gain, high efficiency, and miniaturization for integrating photovoltaic power into a standalone DC microgrid. Reference [4] proposes an averaged small-signal model of a dual-interleaved buck converter using sampler decomposition to include the phase interaction effects that arise from the interleaved sampling of the phase currents. In order to improve stationary characteristics, stability, and transient response, reference [5] proposes a method of modeling and implementation for an interleaved tri-state buck-boost converter. Reference [6] presents a generalized state-space average model for the multi-phase interleaved buck, boost, and buck-boost converters. Using the model, the converter can regulate the system to achieve its maximum efficiency.

Generally, the boost converter system requires specifications such as miniaturization, large power density, high efficiency, a high step-up ratio, fast-tracking performance, and

robust stability. With respect to circuit topology, several methods exist to obtain a high step-up ratio and large power density, such as an interleaved boost converter with coupled inductors and a double-boost converter topology [7–9]. To downsize the system, there are methods to reduce the ripple of input current by applying a multiphase-interleaving method and a multidevice interleaved boost converter [10]. In reference [10], conventional PI controllers are used, and an improvement in the transient response of the output voltage for a load step is reported by applying the interleaving method. However, there is a problem with the responses of the input current and input voltage. As for the control strategy to obtain a fast-tracking performance and robust stability, there are several methods, such as an LMI approach [11], a modified linear quadratic regulator (LQR) [12], and a sliding mode control [13]. For high efficiency, there are methods such as two-phase boost converters with an Electric Double-Layer Capacitor [14,15] and an LQR with a converter loss function [16].

Reference [17] reports a method for downsizing the output filter capacitor by suppressing the output voltage variation with a load current feedforward control for a conventional boost converter. This means that the fast-tracking performance and the disturbance rejection are effective for the miniaturization of a system. From another point of view, the controller needs to handle many variables, such as the output voltage, the input current, and so on, when the converter is connected to the voltage-source three-phase inverters in the HEVs. Generally, the LQR is suitable for multi-input and multi-output systems and is well-known for its fast-tracking performance and complexity for implementation. In reference [18], LQR methods are applied to the grid system. We believe that the LQR is a superior method for establishing a high-tracking performance and downsizing the passive components in power converters. Reference [18], however, requires adding another controller to control the output variables of the converter in addition to the LQR. That leads to more complexity of the control system.

In this paper, in order to improve the complexity of LQR implementation, we propose a novel linear quadratic integral (LQI) control for the interleaved boost converter suitable for HEVs and FCEVs [19]. The proposed method selects the output variables as the output voltage and a current error signal between the two-phase currents, and it can control the output voltage with only the LQI control. To demonstrate the validity of the proposed method, we carry out a comparison verification between the proposed LQI control and conventional PI control because there are a few references for interleaved boost converters with LQI control. For this purpose, steady-state characteristics in the output voltage and the input current are presented. Experimental results demonstrate that the proposed method has a better step response that is ten times faster than that of the PI controller. This article's novelty is applying a novel LQI control to the interleaved boost converter, which can control the output voltage with only the LQI control. The proposed LQI has a simpler control system than conventional LQR and a better tracking performance than conventional PI control. Consequently, this paper contributes not only to an amelioration in the tracking performance and the complexity of implementation but also to the miniaturization of the motor drive system in HEVs and so on. The organization of the paper is as follows. Section 2 describes switching modes using the interleaving method; Section 3 describes the derivation of the small-signal model and the control method of the proposed LQI control; Section 4 presents the steady-state characteristics and transient response of the proposed method. We present a response comparison of the output voltage tracking performance between the proposed LQI and conventional PI controls. The load response comparison is also carried out. Simulation and experimental results demonstrate the superiority of the proposed LQI control. Section 5 describes the conclusions.

2. Interleaved Boost Converter

In this chapter, the basic principle of the interleaved boost converter and its switching mode analysis are introduced [19]. It is assumed that a three-phase voltage-source inverter is combined with the load of the boost converter. However, the inverter is replaced with a

resistor because this paper focuses on the characteristics of the output voltage and input current ripple with the proposed LQI control.

2.1. Circuit Configuration

Figure 1 shows the interleaved boost converter, in which the duty ratios are defined as D_p and D_n given to the switches (S_1 and S_2), respectively. Figure 2 shows the principle of the interleaving method where D is the duty cycle/ratio when D_p and D_n are the same and $D > 0.5$. In Figure 2, the gate signals for the two switches are generated by comparing the duty ratio with two carriers of f_{c1} and f_{c2} that have a 180-phase shift. Here, carrier1 f_{c1} and duty ratio D_p are for S_1, and carrier2 f_{c2} and duty ratio D_n are for S_2, respectively. As a consequence of the interleaving method, the input current amplitude is reduced compared to the phase input current, and the converter produces an input current ripple that has twice the carrier frequency.
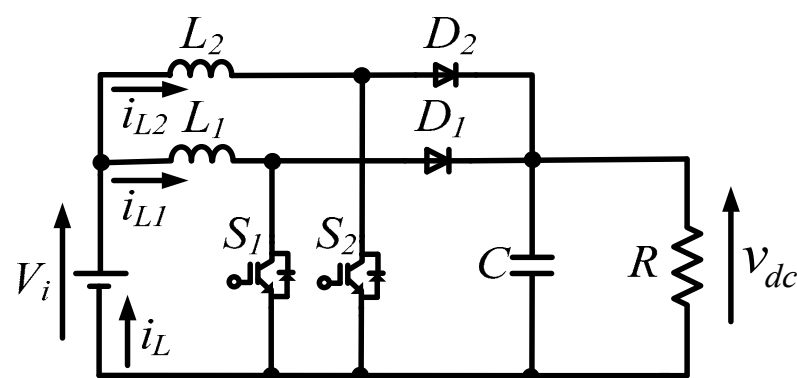
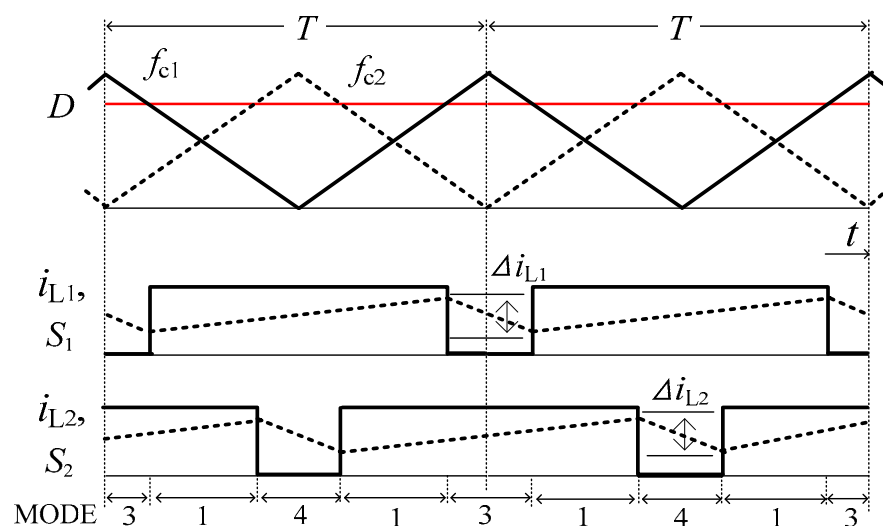**Figure 1.** Interleaved boost converter.

Figure 2. Carriers and switching modes of the interleaving method.

2.2. Switching Modes

Figure 3 shows four modes of the boost converter, which depend on the duty cycle of D. MODE1 is a mode in which both S_1 and S_2 are on, MODE2 is a mode in which both S_1 and S_2 are off, and MODE3 is a mode in which S_1 is off, and S_2 is on. In MODE4, S_1 is on, and S_2 is off. In case $D > 0.5$, in Figure 2, both reactors store the magnetic energy with MODE 1 in Figure 3a. Each reactor boosts the output voltage alternately with MODE 3 in Figure 3c and MODE 4 in Figure 3d.
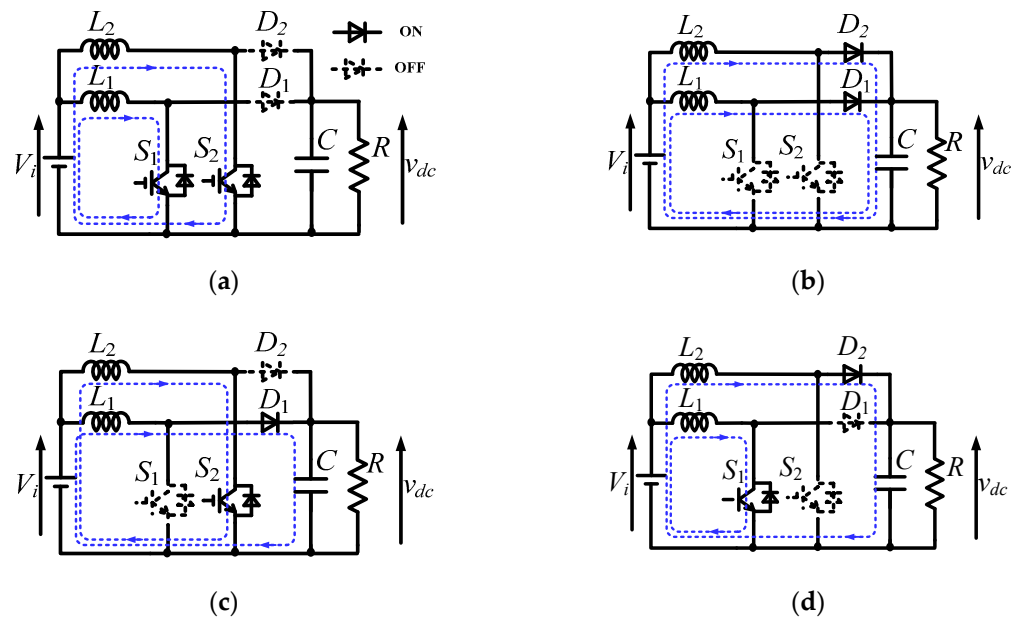
Figure 3. Switching modes of interleaved boost converter. (**a**) MODE1; (**b**) MODE2; (**c**) MODE3; (**d**) MODE4.

3. Control Methods

This chapter describes a theory of the proposed novel linear quadratic integral (LQI) control for the interleaved boost converter. The LQI control controls the output voltage and the balance between two-phase input currents. A small-signal model is demanded for the design of the LQI control. Therefore, the state-space averaging equations are derived. Note that this paper assumes a current continuous mode in the analysis.

3.1. Derivation of State Averaging Equations

Generally, the state space averaging equation and the output equation are expressed as follows:

$$\dot{\boldsymbol{x}}(t) = \boldsymbol{A}\boldsymbol{x}(t) + \boldsymbol{B}\boldsymbol{u}(t) \tag{1}$$

$$\boldsymbol{y}(t) = \boldsymbol{C}\boldsymbol{x}(t) \tag{2}$$

State-space variables are selected as the phase input currents and the output voltage in this paper. Next, state-space equations for the switching modes in Figure 2, in which the duty ratio is $D > 0.5$, are derived. In mathematical modeling, ideal switching elements are assumed for simplifying, but the resistance of a DC reactor is considered. The state-space equation in Mode1 is expressed as the following:

$$\frac{d}{dt}\begin{bmatrix} i_{L1} \\ i_{L2} \\ v_{dc} \end{bmatrix} = \begin{bmatrix} -\frac{r_1}{L_1} & 0 & 0 \\ 0 & -\frac{r_2}{L_2} & 0 \\ 0 & 0 & -\frac{1}{CR} \end{bmatrix} \begin{bmatrix} i_{L1} \\ i_{L2} \\ v_{dc} \end{bmatrix} + \begin{bmatrix} \frac{1}{L_1} \\ \frac{1}{L_2} \\ 0 \end{bmatrix} V_i,$$

$$\dot{\boldsymbol{x}}(t) = \boldsymbol{A}_1\boldsymbol{x}(t) + \boldsymbol{B}_1 V_i \tag{3}$$

The state-space equation in Mode3 is expressed as the following:

$$\frac{d}{dt}\begin{bmatrix} i_{L1} \\ i_{L2} \\ v_{dc} \end{bmatrix} = \begin{bmatrix} -\frac{r_1}{L_1} & 0 & -\frac{1}{L_1} \\ 0 & -\frac{r_2}{L_2} & 0 \\ \frac{1}{C} & 0 & -\frac{1}{CR} \end{bmatrix} \begin{bmatrix} i_{L1} \\ i_{L2} \\ v_{dc} \end{bmatrix} + \begin{bmatrix} \frac{1}{L_1} \\ \frac{1}{L_2} \\ 0 \end{bmatrix} V_i,$$

$$\dot{\boldsymbol{x}}(t) = \boldsymbol{A}_3\boldsymbol{x}(t) + \boldsymbol{B}_3 V_i \tag{4}$$

The state-space equation in Mode4 is expressed as the following:

$$\frac{d}{dt}\begin{bmatrix} i_{L1} \\ i_{L2} \\ v_{dc} \end{bmatrix} = \begin{bmatrix} -\frac{r_1}{L_1} & 0 & 0 \\ 0 & -\frac{r_2}{L_2} & -\frac{1}{L_2} \\ 0 & \frac{1}{C} & -\frac{1}{CR} \end{bmatrix}\begin{bmatrix} i_{L1} \\ i_{L2} \\ v_{dc} \end{bmatrix} + \begin{bmatrix} \frac{1}{L_1} \\ \frac{1}{L_2} \\ 0 \end{bmatrix}V_i,$$

$$\dot{x}(t) = A_4 x(t) + B_4 V_i \tag{5}$$

Coefficient matrices A and B for the state-space equation in Equation (1) are derived by applying the state-space averaging method with A_1, A_3, A_4, B_1, B_3, and B_4, according to Figure 2 [19].

$$A = \begin{bmatrix} -\frac{r_1}{L_1} & 0 & -\frac{\overline{D_p}}{L_1} \\ 0 & -\frac{r_2}{L_2} & -\frac{\overline{D_n}}{L_2} \\ \frac{\overline{D_p}}{C} & \frac{\overline{D_n}}{C} & -\frac{1}{CR} \end{bmatrix}, \qquad B = \begin{bmatrix} \frac{1}{L_1} \\ \frac{1}{L_2} \\ 0 \end{bmatrix} \tag{6}$$

where i_{L1} and i_{L2} are the phase input currents, v_{dc} is the output voltage, V_i is the input voltage, L_1 and L_2 are the inductances of the DC reactors, r_1 and r_2 are the resistances of the DC reactors, C is the capacitance of the output capacitor, and $\overline{D_p} = 1 - D_p$, $\overline{D_n} = 1 - D_n$.

3.2. Derivation of Small-Signal Model

In this section, the linearization of the state-space Equation is carried out since Equation (1) is a nonlinear system. Equation (1) is represented by Equation (6) as the following:

$$\dot{x}(t) = f(x(t), u(t)) = \begin{bmatrix} -\frac{r_1}{L_1}i_{L1} - \frac{\overline{D_p}}{L_1}v_{dc} + \frac{1}{L_1}V_i \\ -\frac{r_2}{L_2}i_{L2} - \frac{\overline{D_n}}{L_2}v_{dc} + \frac{1}{L_2}V_i \\ \frac{\overline{D_p}}{C}i_{L1} + \frac{\overline{D_n}}{C}i_{L2} - \frac{1}{CR}v_{dc} \end{bmatrix} \tag{7}$$

For this purpose, the linearization process with the Jacobian matrix is used in this paper [20]. The state-space equation is linearized around the equilibrium point. The equilibrium point is set as $x(t) = X$, $u(t) = U$. A small-signal model is derived by assuming the fluctuation in the equilibrium point is satisfyingly slower than the carrier period.

$$\frac{d\Delta x(t)}{dt} = \Delta A \Delta x(t) + \Delta B \Delta u(t) \tag{8}$$

$$\Delta A = \left[\frac{\partial f(X, U)}{\partial x(t)}\right]^T = \begin{bmatrix} -\frac{r_1}{L_1} & 0 & -\frac{\overline{D_p}}{L_1} \\ 0 & -\frac{r_2}{L_2} & -\frac{\overline{D_n}}{L_2} \\ \frac{\overline{D_p}}{C} & \frac{\overline{D_n}}{C} & -\frac{1}{CR} \end{bmatrix} \tag{9}$$

$$\Delta B = \left[\frac{\partial f(X, U)}{\partial u(t)}\right]^T = \begin{bmatrix} -\frac{V_{dc}}{L_1} & 0 \\ 0 & -\frac{V_{dc}}{L_2} \\ \frac{I_{L1}}{C} & \frac{I_{L2}}{C} \end{bmatrix} \tag{10}$$

$$x(t) := X + \Delta x(t), \Delta x(t) := \begin{bmatrix} \Delta i_{L1} \Delta i_{L2} \Delta v_{dc} \end{bmatrix}^T$$

$$u(t) := U + \Delta u(t), \Delta u(t) := \begin{bmatrix} \Delta\overline{D_p}, \Delta\overline{D_n} \end{bmatrix}^T$$

$$X := \begin{bmatrix} I_{L1} I_{L2} V_{dc} \end{bmatrix}^T, U := \begin{bmatrix} \overline{D_p}, \overline{D_n} \end{bmatrix}^T$$

where $\overline{D_p} = 1 - D_p$, $\overline{D_n} = 1 - D_n$. The values of the equilibrium point when $D_p = D_n$ are derived as follows:

$$V_{dc} = \frac{V_i}{\overline{D}}, I_{L1} = I_{L2} = \frac{V_i}{2R\overline{D}^2} \tag{11}$$

where $\overline{D} = 1 - D$.

3.3. Derivation of Small-Signal-Model for Servo System

In this section, Equation (8) is extended to be developed as the servo controller so that the output voltage v_{dc} is capable of following the step response, and the phase input currents i_{L1} and i_{L2} are balanced. For this purpose, the output equation, the output variables, and its coefficient matrix are determined as follows:

$$\Delta \boldsymbol{y}(t) = \Delta \boldsymbol{C} \Delta \boldsymbol{x}(t) \tag{12}$$

$$\Delta \boldsymbol{y}(t) := \begin{bmatrix} \Delta v_{dc} \\ \Delta i_L \end{bmatrix}, \quad \Delta \boldsymbol{C} = \begin{bmatrix} 0 & 0 & 1 \\ 1 & -1 & 0 \end{bmatrix}$$

Two expanded state-space variables are introduced to develop the servo system. Additional state-space variables $\omega_1(t)$ and $\omega_2(t)$ are defined as follows.

$$\omega_1(t) := \int_0^t e_1(\tau)d\tau, \quad \omega_2(t) := \int_0^t e_2(\tau)d\tau$$

$$e_1(\tau) := v_{dc\_ref}(\tau) - v_{dc}(\tau), \ e_2(\tau) := \Delta i_{L\_ref}(\tau) - \Delta i_L(\tau)$$

The small-signal model for the servo system can be expressed as follows:

$$\frac{d\boldsymbol{x}_e(t)}{dt} = \Delta \boldsymbol{A}_e \boldsymbol{x}_e(t) + \Delta \boldsymbol{B}_e \boldsymbol{u}_e(t) \tag{13}$$

$$\boldsymbol{x}_e(t) := \begin{bmatrix} \Delta \boldsymbol{x}(t) \boldsymbol{\omega}(t) \end{bmatrix}^T = \begin{bmatrix} \Delta i_{L1} \Delta i_{L2} \Delta v_{dc} \omega_1 \omega_2 \end{bmatrix}^T \tag{14}$$

$$\Delta \boldsymbol{A}_e = \begin{bmatrix} \Delta \boldsymbol{A} & \boldsymbol{O} \\ -\Delta \boldsymbol{C} & \boldsymbol{O} \end{bmatrix}, \quad \Delta \boldsymbol{B}_e = \begin{bmatrix} \Delta \boldsymbol{B} \\ \boldsymbol{O} \end{bmatrix} \tag{15}$$

The system input can be given as the following equation:

$$\boldsymbol{u}_e(t) = \Delta \overline{\boldsymbol{D}} = \boldsymbol{F} \boldsymbol{x}_e(t) \tag{16}$$

where, $\boldsymbol{u}_e(t) = \begin{bmatrix} u_{e1}(t) u_{e2}(t) \end{bmatrix}^T$,

$$\boldsymbol{F} = [\boldsymbol{K}\ \boldsymbol{G}], \ \boldsymbol{K} = \begin{bmatrix} K_1 & K_2 & K_3 \\ K_4 & K_5 & K_6 \end{bmatrix}, \ \boldsymbol{G} = \begin{bmatrix} G_1 & G_2 \\ G_3 & G_4 \end{bmatrix} \tag{17}$$

As shown in Equation (17), feedback gain $\boldsymbol{F}$ consists of the gains $\boldsymbol{K}$ and $\boldsymbol{G}$, in which $\boldsymbol{K}$ is defined as the gain for the state-space variables, and $\boldsymbol{G}$ is for the expanded state-space variables. Therefore, the system input can be represented as the following:

$$\boldsymbol{u}_e(t) = \boldsymbol{K} \Delta \boldsymbol{x}(t) + \boldsymbol{G} \boldsymbol{\omega}(t) \tag{18}$$

where, $\boldsymbol{\omega}(t) = \begin{bmatrix} \omega_1(t) \omega_2(t) \end{bmatrix}^T$. Considering Equations (13)–(18), the configuration of the proposed LQI control is shown in Figure 4. In Figure 4, K_1, K_2, K_3, G_1, and G_2 are the feedback gains for input u_{e1}, and K_4, K_5, K_6, G_3, and G_4 are the feedback gains for input u_{e2}. These feedback gains are obtained by solving the Riccati algebraic equation as explained in Equation (20). In the theory of optimal control, the performance index so that the system is stable is described as the following equations:

$$J = \int_0^\infty \{x_e(t)^\mathsf{T} Q x_e(t) + u_e(t)^\mathsf{T} R u_e(t)\} dt \tag{19}$$

where, Q is a non-negative definite symmetric matrix, which is the weight coefficient matrix for each state-space variable, and R is a positive definite matrix, the weight coefficient matrix for the control input. The weight coefficient matrices Q and R of the LQI control are set as Q = diag $[q_1, q_2, q_3, q_4, q_5]$ and R = diag $[r_1, r_2]$, in which diag denotes a diagonal matrix. Each coefficient of the weight coefficient matrices Q and R corresponds to $q_1:i_{L1}$, $q_2:i_{L2}$, $q_3:v_{dc}$, $q_4:\omega_1$, $q_5:\omega_2$, $r_1:\overline{D_p}$, and $r_2:\overline{D_n}$. The feedback gain F can be given as the following:

$$F = -R^{-1} \Delta B_e^\mathsf{T} P \tag{20}$$

where, the matrix P is the positive definite symmetric matrix that satisfies the Riccati algebraic equation as the following.

$$P \Delta A_e + \Delta A_e^\mathsf{T} P - P \Delta B_e R^{-1} \Delta B_e^\mathsf{T} P + Q = 0 \tag{21}$$
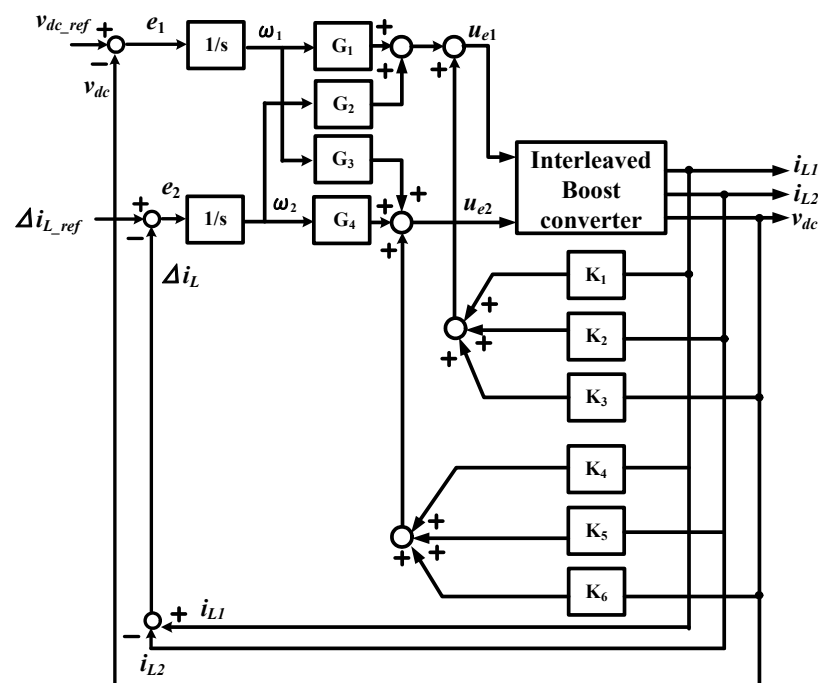
Figure 4. Configuration of LQI control.

3.4. PI Controller

This section investigates the configuration of the PI controller for comparison with the proposed method. Figure 5 shows the configuration of the PI control system. The PI control system consists of a major loop of voltage control and a minor loop of current control, which has two PI controllers so as to control each phase's input current [19].
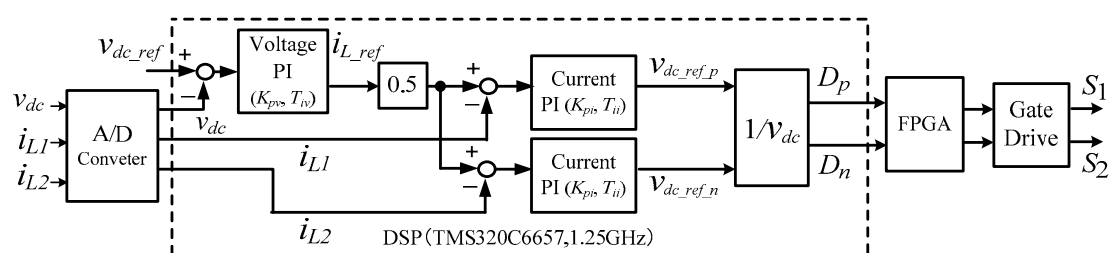

Figure 5. Configuration of PI control.

4. Verification

Figure 6 shows the experimental setup. The experiment was carried out with a prototype converter with a rated power of 700 W. For controllers, the PE-Expert4 is used, which consists of a DSP board (TMS320C6657), an FPGA board (MWPE4-IPFPGA-24), an AD board (AD7357, 14-bit), and a DA board (AD5547,16-bit). Table 1 shows the parameters of the main circuit. The prototype has snubber circuits with a resistance of 1 kΩ and a capacitance of 1nF for compensating the effect of parasitic inductances. In this paper, the weight coefficients in Equation (19) are designed through simulations [19]. The "Arimoto-Potter method", used to solve Riccati algebraic equations and gains using the Hamiltonian matrix, is employed for gain calculation. Table 2 shows the gains designed. On the other hand, the PI control parameters were determined using Bode diagrams and simulations. The simulation of the PI controller was carried out to ensure stable control of the input current. As a result, a control bandwidth for the current control system was designed at 1000 rad/s. The control bandwidth of the voltage control was designed at 1/10 of that of the current control. Table 3 shows the parameters of the PI control. The software used for simulation is the PSIM 64-bit ver.11.1.7. In the simulation, ideal switching models are used for IGBTs and Diodes, and the parasitic inductance is not considered for simplification.
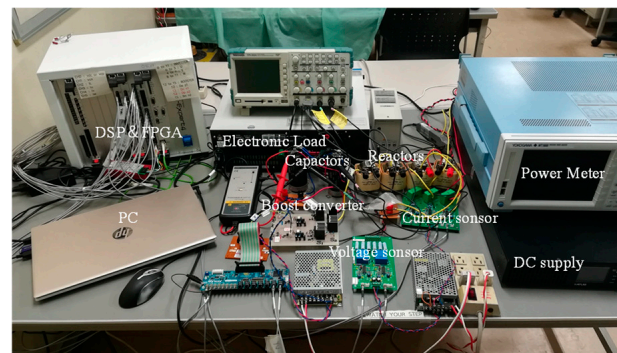

Figure 6. Experimental setup.

Table 1. Circuit conditions.

Input voltage V_i	100 V
Carrier frequency f_{c1} and f_{c2}	20 kHz
IGBT rated voltage rated current	FGH40T120SMD 1200 V 40 A
Diode rated voltage rated current	FEP16DT 600 V 16 A
Load (Resistance) R	100 Ω
DC reactor inductance L_1 and L_2 rated current core resistance r_1 and r_2	- 1.8 mH 9 A silicon steel plate 68.6 mΩ
Capacitance C	750 μF
Converter Power rating Output voltage V_{dc} Duty cycle Input current Output current	- 700 W 250 V 0.6 7 A 2.8 A

Table 2. The parameters of LQR for Q = diag [1, 10, 0, 100,000, 100,000] and R = diag [1, 1].

	Feedback Gain		
K_1	2.2138	K_6	1.9795
K_2	1.1652	G_1	−497.60
K_3	2.0918	G_2	−97.733
K_4	1.1604	G_3	−478.74
K_5	2.1158	G_4	106.94

Table 3. Parameters of PI controllers.

Parameter	Value
K_{pv}	0.15
T_{iv}	0.02
K_{pi}	4.0
T_{ii}	0.002

4.1. Steady-State Characteristics

Figure 7 shows the steady-state characteristics of the output voltage, the input current, and the phase input current when the reference voltage is 150 V. Figure 7a,b are the simulated and experimental results, respectively. It can be seen that the output voltage is controlled to its reference value, the input current ripple is reduced, and its frequency is twice the carrier frequency, 40 kHz. Figure 8 shows the steady-state characteristics when the reference voltage is 200 V and the duty ratio is 0.5. In this condition, the input current ripple is approximately zero. Similarly, Figure 9 shows the characteristics when the reference voltage is 250 V. The ripples of input current and phase input current for simulation are 0.53 A and 1.53 A, respectively. On the other hand, those values for the experiment are 0.6 A and 1.57 A, respectively. Figures 7–9 show that the simulated results agree well with the experimental results.
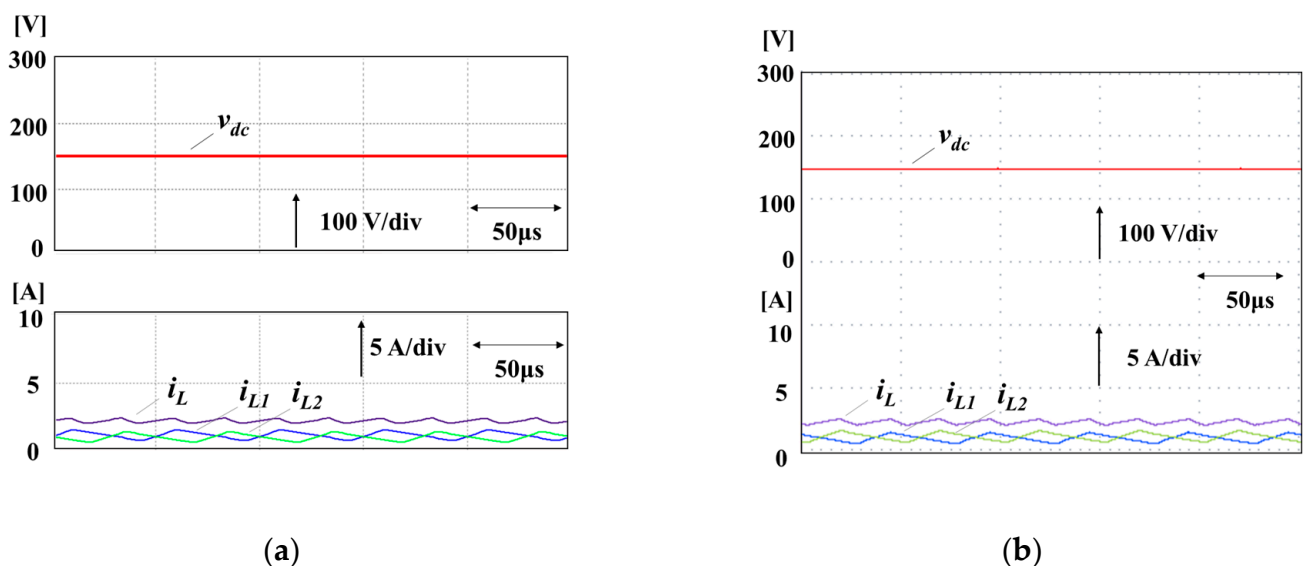
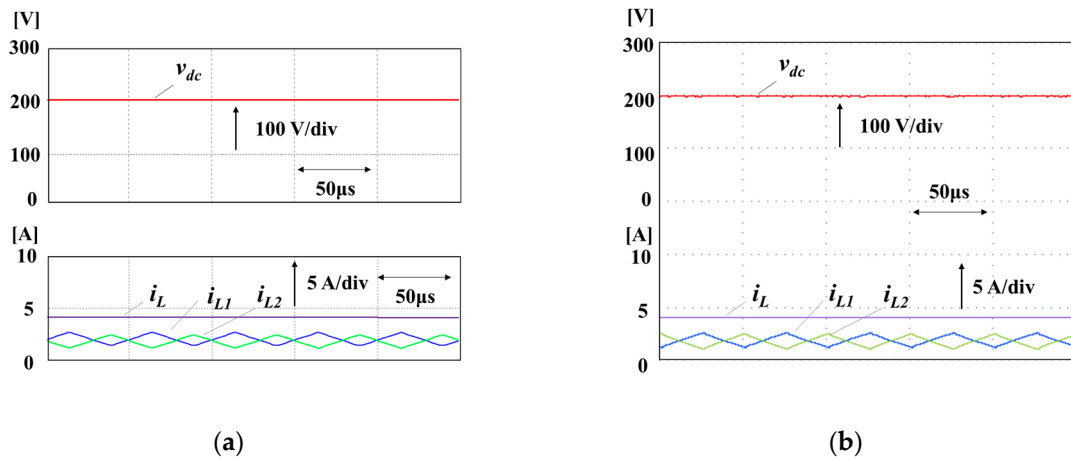**Figure 7.** Steady state characteristics (v_{dc_ref} = 150 V). (**a**) Simulated result; (**b**) Experimental result.

Figure 8. Steady state characteristics (v_{dc_ref} = 200 V). (**a**) Simulated result; (**b**) Experimental result.
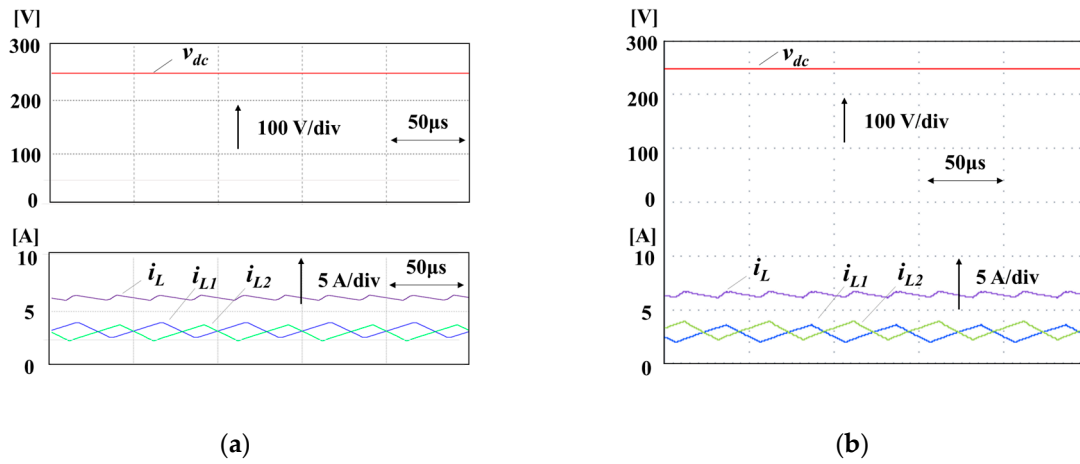

Figure 9. Steady state characteristics (v_{dc_ref} = 250 V). (**a**) Simulated result; (**b**) Experimental result.

4.2. Tracking Performance and Load Response

Figure 10 shows the simulated results of the tracking performance of the output voltage, in which the reference voltage changes in steps from 150 V to 190 V. In the experiment, the step voltage was chosen so that the parasitic inductance between the input voltage and the load does not affect the output voltage response. Because the value of the parasitic inductance is very small with μH, and its time constant is sufficiently smaller than that of output voltage, its effect is very small. The higher the output voltage, the output voltage response of the converter has a large influence. However, the experiment was carried out on the condition that the parasitic inductance does not affect the output voltage response. Figure 10a,b are the results of the proposed method and the PI control, respectively. In case Figure 10a, the output voltage reaches its reference value in about 10 ms, while that of the PI control reaches about 80 ms. Figure 11 shows the experimental results in the same condition as Figure 10. The tracking performance is 10 ms, which is the same as the simulation, while that of the PI control is about 100 ms, which is a little longer than that of the simulation due to an overshoot. The proposed method has a ten times faster tracking performance than the PI control. Figure 12 shows the load response when the load is changed from 200 W to 500 W. Figure 12a,b are the results of the proposed method and the PI control, respectively. In Figure 12b, the output voltage drops by a maximum of about 10 V and fluctuates for 70 ms. On the other hand, in Figure 12a, the output voltage keeps a constant value without fluctuation. Figure 13 shows the response when the load changes from 500 W to 200 W. In Figure 13b, the output voltage rises about 10 V and varies over 70 ms. Figure 13a shows that the output voltage keeps a constant

value without fluctuation. The experimental results demonstrate that the proposed method has an excellent disturbance rejection for a load step response compared to the PI control. In the experiment, the buttery and the capacitor have slight voltage variations because we assume the converter has a relatively stable voltage source. The variation of the voltage source affects a disturbance in the control system. If the voltage source is unstable, the converter system will likely have a serious influence, such as input current ripple distortion, an imbalance between two-phase input currents, output voltage variation, and delayed output voltage response.
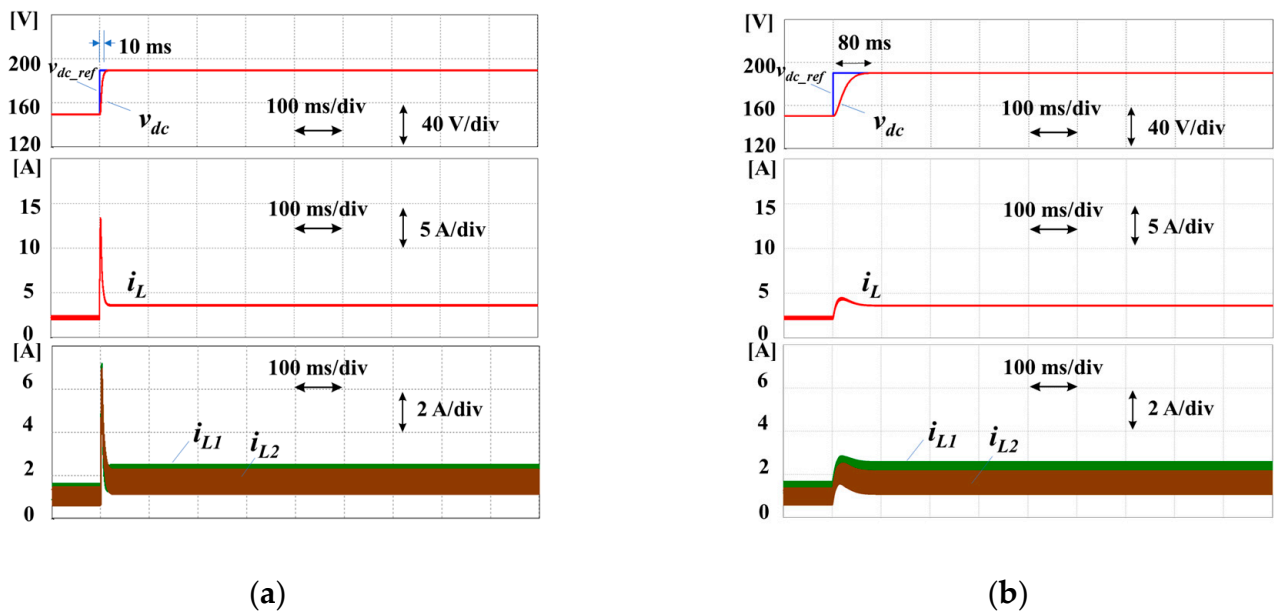
Figure 10. Simulated results of tracking performance (150 V to 190 V). (**a**) LQI control; (**b**) PI control.
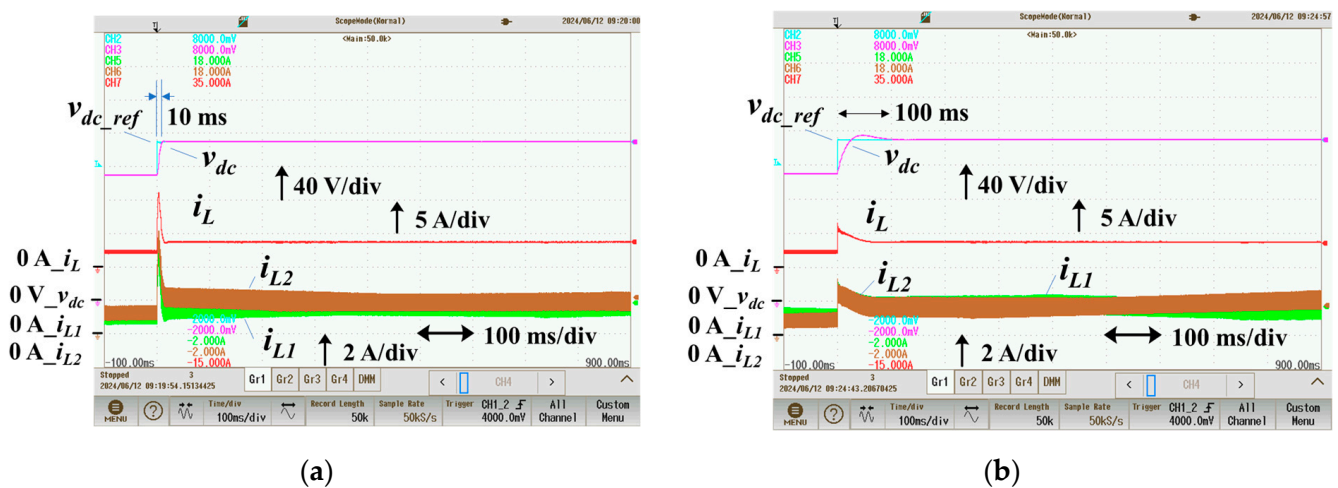
Figure 11. Experimental results of tracking performance (150 V to 190 V). (**a**) LQI control; (**b**) PI control.
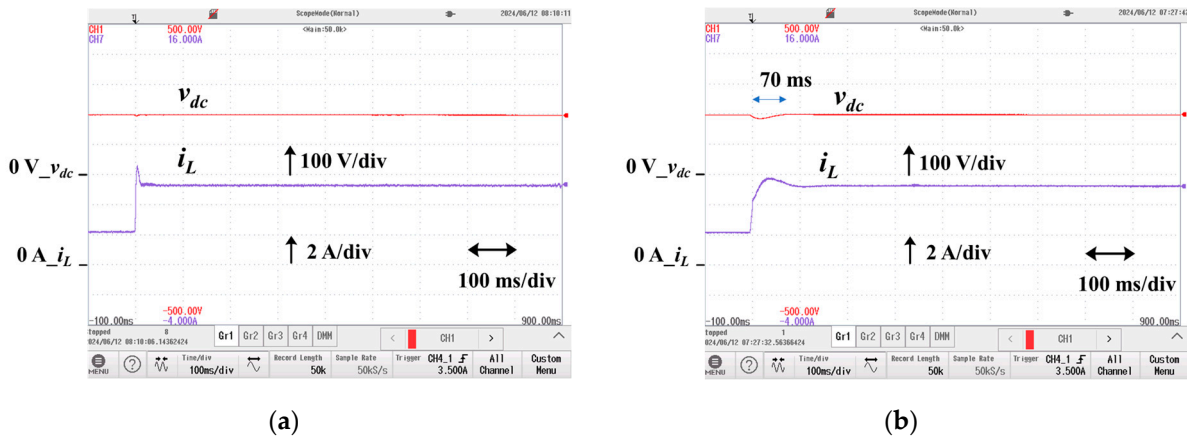
Figure 12. Experimental results of load response (200 W to 500 W). (**a**) LQI control; (**b**) PI control.
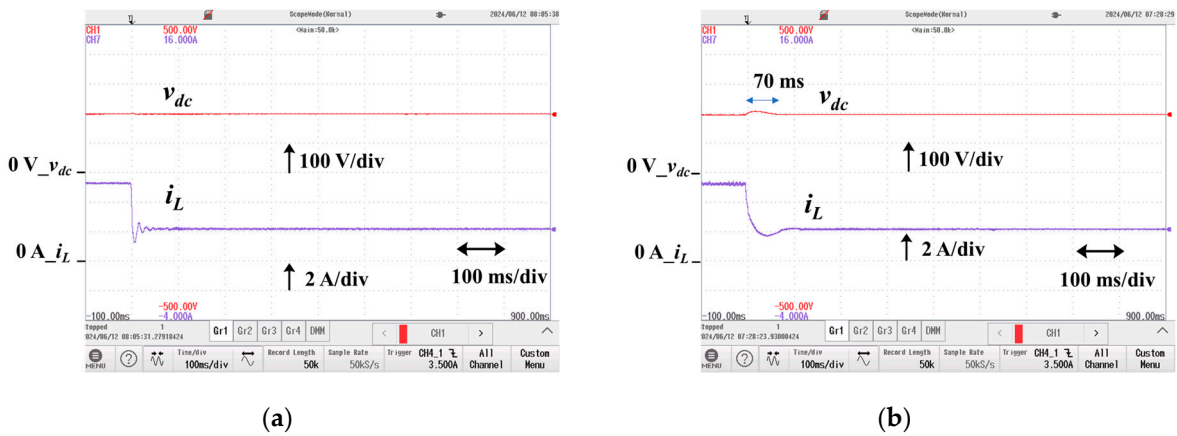

Figure 13. Experimental results of load response (500 W to 200 W). (**a**) LQI control; (**b**) PI control.

5. Conclusions

This paper proposed a novel linear quadratic integral (LQI) control for the interleaved boost converters suitable for HEVs and FCEVs. The conclusions obtained in this paper are as follows:

i. The small-signal model for the servo system of the interleaved-boost converter was derived. The LQI control was proposed using the small-signal model.

ii. In the proposed method, an output voltage and a current signal error between two-phase input currents are selected as output variables to control the output voltage and balance between two-phase input currents. The proposed method has a simple system and can control both output variables without additional controllers.

iii. Steady-state characteristics in terms of the output voltage and the input current were demonstrated by experiments and simulations using an experimental apparatus with a rated power of 700 W.

iv. The validity of tracking performance and load response of the proposed method was demonstrated by comparing it with that of the conventional PI control. The tracking performance of the LQI control for the 40 V step response has a ten times faster response than that of the PI control. Also, the experimental results demonstrated that the proposed method can keep the output voltage constant for a load step of 300 W while that of the PI control varies by 10 V during 70 ms and has an excellent disturbance rejection.

v. Therefore, the proposed LQI control improves the tracking performance and the load response and miniaturizes the motor-drive systems in HEVs and FCEVs.

For future research, current sharing control in the interleaved boost converters using the proposed LQI control is considered for a multi-buttery management system combined with an electric double-layer capacitor and fuel-cell battery.

Data Availability Statement: The original contributions presented in the study are included in the article, further inquiries can be directed to the corresponding author.

Conflicts of Interest: The authors declare no conflict of interest.

References

1. Mizutani, M.; Tachibana, T.; Morimoto, M.; Akatsu, K.; Hoshi, N. Electric Drive Technologies Contributing to Low-Fuel-Consumption Vehicles. *IEEJ Trans. Ind. Appl.* **2015**, *135*, 884–891. (In Japanese) [CrossRef]
2. Yamamoto, K.; Shinohara, K. Characteristics of Permanent-Magnet Synchronous Motor Driven by PWM Inverter with Voltage Booster. *IEEE Trans. Ind. Appl.* **2004**, *40*, 1145–1152. [CrossRef]
3. Singh, K.A.; Prajapati, A.; Chaudhary, K. High-Gain Compact Interleaved Boost Converter with Reduced Voltage Stress for PV Application. *IEEE J. Emerg. Sel. Top. Power Electron.* **2022**, *10*, 4763–4770. [CrossRef]
4. Villarruel-Parra, A.; Forsyth, A.J. Modeling Phase Interactions in the Dual-Interleaved Buck Converter Using Sampler Decomposition. *IEEE Trans. Ind. Electron.* **2019**, *66*, 3316–3322. [CrossRef]
5. Rana, N.; Banerjee, S.; Giri, S.K.; Trivedi, A.; Williamson, S.S. Modeling, Analysis and Implementation of an Improved Interleaved Buck-Boost Converter. *IEEE Trans. Circuits Syst. II: Express Briefs* **2021**, *68*, 2588–2592. [CrossRef]
6. Azer, P.; Emadi, A. Generalized State Space Average Model for Multi-Phase Interleaved Buck, Boost and Buck-Boost DC-DC Converters: Transient, Steady-State and Switching Dynamics. *IEEE Access* **2020**, *8*, 77735–77745. [CrossRef]
7. Henn, G.A.L.; Silva, R.N.A.L.; Praça, P.P.; Barreto, L.H.S.C.; Oliveira, D.S., Jr. Interleaved-Boost Converter with High Gain. *IEEE Trans. Power Electron.* **2010**, *25*, 2753–2761. [CrossRef]
8. Dai, Z.; Liu, J.; Li, K.; Mai, Z.; Xue, G. Research on a Modeling and Control Strategy for Interleaved Boost Converters with Coupled Inductors. *Energies* **2023**, *16*, 3810. [CrossRef]
9. Liu, Z.; Du, J.; Yu, B. Design Method of Double-Boost DC/DC Converter with High Voltage Gain for Electric Vehicles. *World Electr. Veh. J.* **2020**, *11*, 64. [CrossRef]
10. Hegazy, O.; Mierlo, J.V.; Lataire, P. Analysis, Modeling, and Implementation of a Multidevice Interleaved DC/DC Converter for Fuel Cell Hybrid Electric Vehicles. *IEEE Trans. Power Electron.* **2012**, *27*, 4445–4458. [CrossRef]
11. Olalla, C.; Leyva, R.; Aroudi, A.E.; Queinnec, I. Robust LQR Control for PWM Converters: An LMI Approach. *IEEE Trans. Ind. Electron.* **2009**, *56*, 2548–2558. [CrossRef]
12. Agrawal, N.; Samanta, S.; Ghosh, S. Modified LQR Technique for Fuel-Cell-Integrated Boost Converter. *IEEE Trans. Ind. Electron.* **2021**, *68*, 5887–5896. [CrossRef]
13. Huangfu, Y.; Zhuo, S.; Chen, F.; Pang, S.; Zhao, D.; Gao, F. Robust Voltage Control of Floating Interleaved Boost Converter for Fuel Cell Systems. *IEEE Trans. Ind. Appl.* **2018**, *54*, 665–674. [CrossRef]
14. Marchesoni, M.; Vacca, C. New DC-DC Converter for Energy Storage System Interfacing in Fuel Cell Hybrid Electric Vehicles. *IEEE Trans. Power Electron.* **2007**, *22*, 301–308. [CrossRef]
15. Yamamoto, K.; Imakiire, A.; Iimori, K. PWM Inverter with Voltage Boosters with Regenerating Capability Augmented by Electric Double-Layer Capacitor. *IEEJ Trans. Ind. Appl.* **2011**, *131*, 671–678. (In Japanese) [CrossRef]
16. Neacsu, D.O.; Sirbu, A. Design of a LQR-Based Boost Converter Controller for Energy Savings. *IEEE Trans. Ind. Electron.* **2020**, *67*, 5379–5388. [CrossRef]
17. Takei, D.; Fujimoto, H.; Hori, Y. Load Current Feedforward Control of Boost Converter for Downsizing the Output Filter Capacitor. *IEEJ Trans. Ind. Appl.* **2015**, *135*, 457–466. (In Japanese) [CrossRef]
18. Rivera, G.H.V.; Amaya, I.; Duarte, J.M.C.; Bayliss, J.C.O.; Cervantes, J.G.A. Hybrid Controller Based on LQR Applied to Interleaved Boost Converter and Microgrids under Power Quality Events. *Energies* **2021**, *14*, 6909. [CrossRef]
19. Sakasegawa, E.; Chishiki, R.; Sedutsu, R.; Soeda, T.; Haga, H.; Kennel, R.M. Comparison of Interleaved Boost Converter and Two-Phase Boost Converter Characteristics for Three Level Inverters. *World Electr. Veh. J.* **2023**, *14*, 7. [CrossRef]
20. Gao, L. Alternative Way to Develop Small-Signal Models of Power Converters. *IEEE Trans. Power Electron. Mag.* **2024**, *11*, 62–69.